

Kinetic grain growth, shape memory and corrosion behavior of two Cu-based shape memory alloys after thermomechanical treatment

Ahmad Ostovari MOGHADDAM, Mostafa KETABCHI, Reza BAHRAMI

Department of Mining and Metallurgical Engineering, Amirkabir University of Technology, Tehran, Iran

Received 13 September 2012; accepted 13 December 2012

Abstract: Metallurgical and mechanical properties along with shape memory and corrosion behavior of Cu–11.8% Al–3.7% Ni–1%Mn and Cu–11% Al–5.6% Mn shape memory alloys (SMAs) were comparatively studied. The influence of grain refinement on the properties was studied by optical microscopy (OM), scanning electron microscopy (SEM), differential scanning calorimetry (DSC), potentiodynamic polarizations and bend and tensile tests. Static recrystallization and kinetic grain growth show a rapid recrystallization in the first 15 s of annealing at 800 °C followed by grain growths. The minimum grain sizes obtained after 15 s are 90 and 260 μm for Cu–Al–Ni–Mn and Cu–Al–Mn, respectively. Tensile tests show typical three-stage curves for both alloys, and it is seen that alloys exhibit high fracture stress and strain after grain refinement. Microstructural observations show zig-zag morphology of β'_1 martensite in the Cu–Al–Ni–Mn and coexistence of β'_1 and γ'_1 in the Cu–Al–Mn, which were confirmed by differential scanning calorimetry results. The shape memory ratios (η) of the alloys before thermomechanical treatment, and after thermomechanical annealing at 800 °C for different time up to 15 min followed by water quenching, were evaluated. In addition, corrosion behavior of alloys after grain refinement was analyzed by means of potentiodynamic polarization measurements. The results showed that the anodic reactions were dominated by dissolution of copper, and Cu–Al–Ni–Mn alloy exhibits a better corrosion resistance than Cu–Al–Mn alloy.

Key words: shape memory alloys (SMAs); grain refinement; corrosion; shape memory properties

1 Introduction

Shape memory effect (SME) and superelasticity (SE) are unique properties that proceed by thermoelastic martensitic transformation. During last decades, practical application of shape memory alloys have been progressively increased in numerous applications, such as actuators, sensors, coupling, smart systems, materials with high damping capacity, structural and medical applications [1–3]. Among the numerous shape memory alloys (SMAs), Cu-based SMAs because of their lower cost and acceptable SME and SE compared with other SMAs, raised as the most attractive alloy for practical exploitations. But many potential applications of Cu-based SMAs are restricted by brittleness nature of these alloys. The brittleness of the β -polycrystalline Cu-based alloys is due to the B_2 , DO_3 and $L2_1$ ordered structure of parent β -phase and abnormally high elastic anisotropy ($A=2C_{44}/(C_{11}-C_{12})=13$ and 15 for Cu–Al–Ni and Cu–Al–Zn SMAs, respectively, where C_{ij} is the

elastic stiffness) which leads to stress concentration at grain boundaries [4]. The typically large grain sizes of the β -phase in these alloys intensify this tendency to brittleness even further [4]. Many attempts have been made to improve the mechanical properties of these alloys, especially, Cu–Al–Ni SMA, through grain refinement by thermomechanical treatment [5–7] and addition of alloying elements [8,9].

Recent studies showed that Cu–Al–Mn SMAs with Al content lower than 18% (mole fraction) and Mn content higher than 8% possess good ductility which is attributed to the low degree of order in the parent phase with $L2_1$ structure [10]. Two types of order-disorder transitions, $\beta(A_2)\rightarrow\beta_2(B_2)$ and $\beta_2(B_2)\rightarrow\beta_1(L2_1)$, occur during quenching in β region. In composition range above 16% Al, $L2_1\rightarrow\beta'_1(6M)$ martensitic transformation occurs, while in composition range below 16% Al the transition from A_2 to $L2_1$ is suppressed by quenching and the A_2 phase martensitically transforms to the $\gamma'_1(2M)$ structure [10,11]. Recently, SUTOU et al [11] investigated the effect of thermomechanical treatment

and Ni addition on the SE of Cu–Al–Mn SMAs. The thermomechanical treatment included annealing in the FCC (α)+BCC(β) two-phase region, followed by heavy cold reduction which dominated the $\{1\ 1\ 2\}\langle 110\rangle$ recrystallization texture. The final grain sizes were 200 μm to 400 μm which were dependent on the Ni content, and SE strain of 7% was achieved in the textured sheets. Effect of aging [12,13] and alloying element [14,15], as well as damping properties [16–18] and martensite phases [19] in Cu–Al–Mn systems have been studied very well, but till now no reports are available on corrosion behavior of Cu–Al–Mn SMAs.

In this work, in order to obtain grain refinement of Cu–Al–Mn and Cu–Al–Ni–Mn SMAs, a thermo-mechanical treatment was used, and microstructure, kinetic grain growth, corrosion behavior, mechanical and shape memory properties of these alloys were comparatively studied.

2 Experimental

2.1 Alloy preparation

Two kinds of Cu-based SMAs, Cu–Al–Mn (AMD1) and Cu–Al–Ni–Mn (AMD2) alloys were prepared by induction melting of commercially pure Cu, Al plates and Ni, Mn powders in a graphite crucible under normal atmosphere. Glass was used as a slag to reduce the oxidation. Each ingot was remelted two times and poured

in the cast iron mould with dimensions of 10 cm×5 cm×3 cm. An ice mold was placed under the cast iron mold to act as a chill and lead the shrinkage porosities to the surface of ingots. This region was then cut from the ingots. The cast ingots were homogenized at 850 °C for 12 h, and quenched in room temperature water. Chemical compositions of prepared alloys were determined by electron dispersion spectroscopy (EDS) and are listed in Table 1.

2.2 Thermomechanical treatment and characterization

Because of low cold workability of Cu–Al–Ni-based alloys, a special thermomechanical treatment was used for grain refinement of these alloys. The thermomechanical treatment was carried out. The cast ingot was hot rolled at 850 °C to a final thickness of 2 mm in 7 passes and quenched immediately after the final hot rolling pass to suppress recrystallization [5]. After 7 passes of rolling at 850 °C, the alloy temperature is still high enough and recrystallization may be occurred. So, the alloy must be quenched immediately after the final hot rolling pass to prevent recrystallization. Several specimens were prepared from the 2 mm-thick plate obtained in the first step, recrystallized at 800 °C for different time, and then quenched in room temperature water. The mean β grain size of the alloys was determined by an optical microscope (OM) and a linear intercept method [20], As shown in Fig. 1, the mean

Table 1 Chemical compositions, transformation temperatures and tensile properties of recrystallized AMD1 and AMD2 alloys

| Alloy | w/% | | | | $A_s/^\circ\text{C}$ | $A_f/^\circ\text{C}$ | $M_s/^\circ\text{C}$ | $M_f/^\circ\text{C}$ | $\sigma_{0.2}/\text{MPa}$ | σ_f/MPa | $\varepsilon_f/\%$ |
|-------|------|------|-----|-----|----------------------|----------------------|----------------------|----------------------|---------------------------|-----------------------|--------------------|
| | Cu | Al | Ni | Mn | | | | | | | |
| AMD1 | 83.4 | 11 | – | 5.6 | 49 | 102 | 78 | 40 | 155±5 | 530 | 11 |
| AMD2 | 83.5 | 11.8 | 3.7 | 1 | 80 | 146 | 122 | 71 | 170±5 | 620 | 11 |

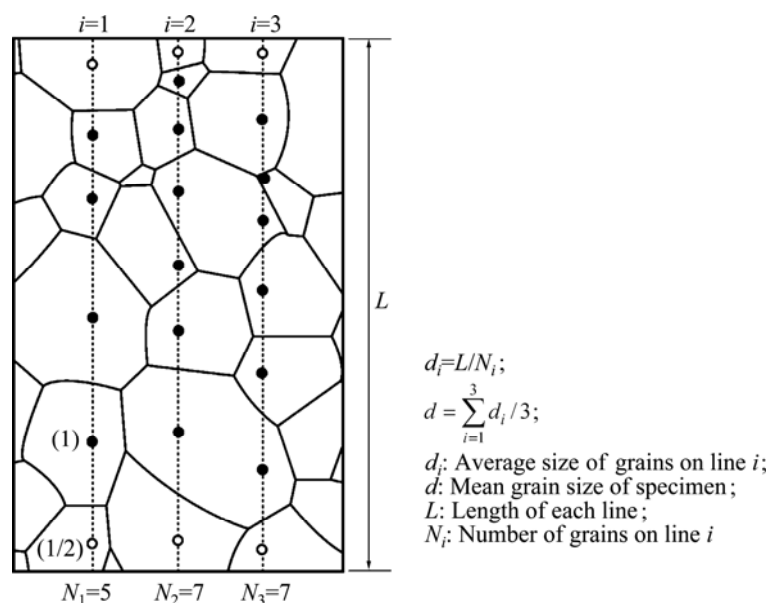


Fig. 1 Schematic diagram for calculation of mean grain size (Grains indicated by open circles were counted as 1/2 [20])

grain size of the alloys can be calculated from the average of grains on three lines.

The SME of the specimens recrystallized at 800 °C for different time was measured by bending tests. As shown in Fig. 2, each specimen at room temperature was bent to φ° around a circular cylinder of 50 mm in diameter, and then heated above the A_f for shape recovery. The residual angles θ were then measured. The maximum deformation strain, ε , and the shape recovery ratio η in this process can be calculated using the following equations:

$$\varepsilon=t/(D+t) \quad (1)$$

$$\eta=(1-\theta/\varphi)\times 100\% \quad (2)$$

where t is the specimen thickness; D is the diameter of the cylinder; φ and θ are the bent angle and residual angle after shape recovery, respectively. In this work, $t=2$ mm, and $D=50$ mm. So, the specimens subjected to a strain (ε) of 3.8%.

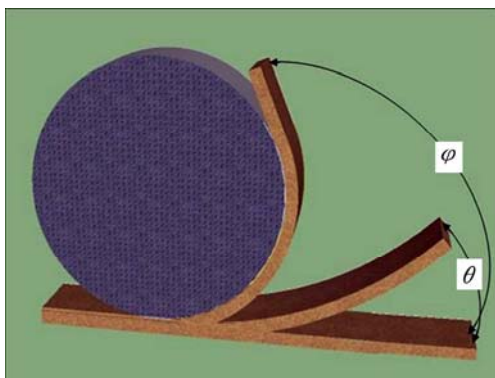


Fig. 2 Schematic illustration of measurement of shape memory ratio

The samples were prepared for SEM by mechanical grinding and etching in a solution composed of 5 g FeCl_3 , 30 mL HCl and 100 mL H_2O . Forward- and reverse-martensitic transformation temperatures were determined by a toledo mettler differential scanning calorimeter (DSC) with a heating/cooling rate of 10 °C/min at 0–200 °C. Tensile test was conducted on specimens at room temperature by a Instron 8502 testing machine operated at a constant strain rate of 2.1×10^{-3} s^{-1} .

The electrochemical studies were performed in a typical three-electrode cell using an AUTOLAB-PGSTAT30 Potentiostat/Galvanostat. The platinum sheet and Ag/AgCl were used as counter electrode and reference electrode, respectively. The cubic working electrodes were prepared by cutting the recrystallized AMD1 and AMD2 alloys into 3 mm \times 2 mm \times 0.2 cm sheets and covering them by Teflon to expose a square area of 1 cm^2 to the electrolyte. All experiments were carried out in a cell containing 100 mL 5 g NaCl (ie, 5% NaCl solution) at 25 °C. Before potentiodynamic and

linear polarization measurements, the working electrodes were wet ground with different grit emery papers, rinsed in acetone, washed in distilled water, and finally, submerged into the electrochemical solution.

3 Results and discussion

3.1 Microstructure and kinetic grain growth

Figure 3 shows the variation of average grain size with recrystallization time at 800 °C for AMD1 and AMD2 alloys. The initial grain sizes of the hot-rolled AMD1 and AMD2 alloys were 1020 and 620 μm , respectively. The curves can be divided into two stages: a quick recrystallization region which occurred in the first 15 s and successive grain growth region with increasing solution treatment time. The minimum grain sizes, which were obtained after recrystallization for 15 s, were 260 and 90 μm for AMD1 and AMD2 alloys, respectively. Initial and typical microstructures after completion of the recrystallization for both alloys are shown in Fig. 4. It is seen from Figs. 4 that the hot-rolled alloys have a coarse-grained structure, whereas the alloys after recrystallization possess a fine-grained structure, and the grain size of AMD2 is smaller than that of AMD1 alloy. This smaller grain size is common in systems with impurities due to grain boundary pinning effect by dispersed particles. So, in order to obtain grain refinement this thermomechanical treatment is more effective for AMD2 alloy. Nevertheless, it is shown that addition of alloying elements such as Ni, B and Cr is very effective in the grain refinement of Cu–Al–Mn SMAs [11,16].

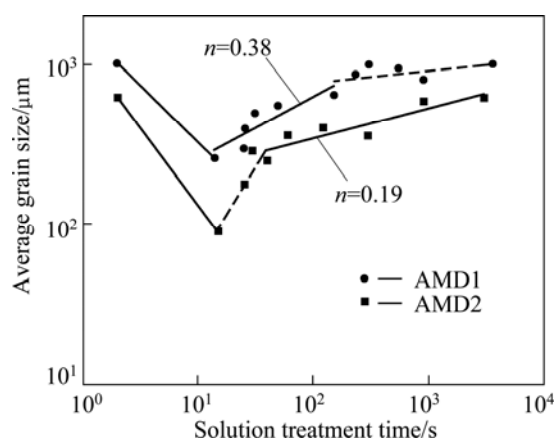


Fig. 3 Variations of grain size vs solution treatment time at 800 °C for AMD1 and AMD2 alloys (n is the kinetic exponent)

Grain growth kinetics of these alloys obeys Hillert distribution. According to Hillert distribution, the difference between the maximum grain size and 1.8 times the average grain size is smaller than zero [21]. This means that grain growth occurs uniformly

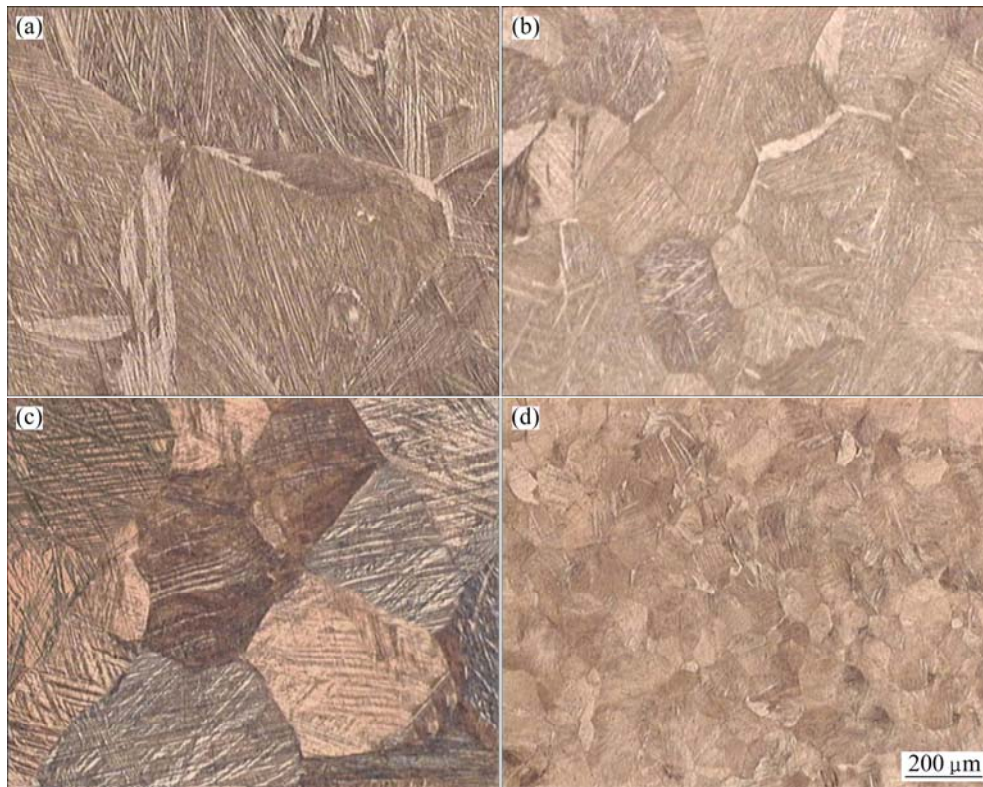


Fig. 4 Optical micrographs of AMD1 alloy before recrystallization (a), AMD1 alloy after recrystallization (b), AMD2 alloy before recrystallization (c) and AMD2 alloy after recrystallization (d)

throughout the specimens and the grain size distribution follows an asymptotic law. Such kinetics obeys Burke and Turnbull model [21]. For AMD1 alloy, the kinetics of grain growth can be formulated by a type of Burke and Turnbull model, $D=kt^{0.38}$, where D is the grain size, and k is a constant. The deviation from the power law at higher grain sizes can be explained by the well-known sheet thickness effect [5,6]. This is a usual grain growth behavior during heat treatment. In the case of AMD2 alloy, a different grain growth behavior is observed, namely, a rapid grain growth period occurred in the first 50 s followed by a normal grain growth. This abnormal behavior can be explained that during hot rolling stage, temperature drops to around 750 °C, and at this temperature a second phase (γ_2) is precipitated at the grain boundaries [5]. When this structure was annealed at 800 °C, in the initial seconds of recrystallization, the presence of precipitates caused a delay in the grain growth so that after 15 s the grain size in the range of 80–100 μm is obtained. However, with increasing solution treatment time, grain growth as well as precipitate dissolution takes place (rapid grain growth region). After about 40 s precipitates are completely dissolved, a single beta phase is obtained and the normal grain growth region is dominated. The slope of the fitted line in the normal grain growth region (Fig. 3) is 0.19 and this is corresponding to the theoretical grain growth

equation, $D=kt^{0.19}$. Lower exponent of AMD2 alloy, as discussed above, may be a result of solute (Mn) drag effect at grain boundaries.

3.2 Mechanical properties

Figure 5 shows the stress—strain curves obtained by tensile test at room temperature for AMD1 and AMD2 alloys before and after recrystallization treatment. Both alloys after recrystallization exhibit significantly higher fracture stress, σ_f , and strain, ϵ_f , compared with coarse grain as-rolled alloys. In particular, recrystallized AMD2 alloy, which has the finest grain size, also possesses the higher fracture stress compared with other alloys.

The fracture strength after recrystallization was increased from 390 MPa to about 530 MPa for AMD1 alloy, and from 430 MPa to about 620 MPa for AMD2 alloy. In addition, the fracture strain was increased from 9% to 11% and 8% to 11% for AMD1 and AMD2 alloys, respectively. It is obvious that the grain refinement affects the stress—strain behavior of alloys. As the grain size decreases, the free space of dislocations slide before interaction with grain boundaries is also decreased, and thus, strain hardening occurs. The stress—strain behavior is also influenced by other factors such as degree of order and type of thermally induced martensite [22]. Increasing solution treatment time causes ordering in these alloys and dislocation movement

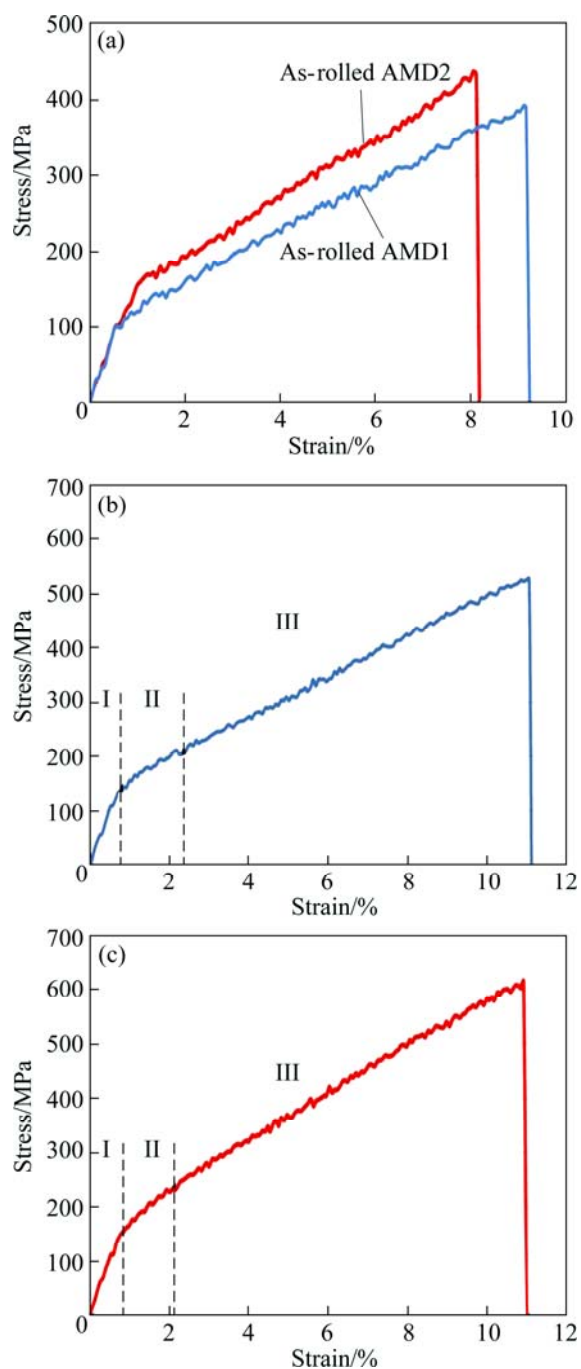


Fig. 5 Stress—strain curves for AMD1 and AMD2 alloys before recrystallization (a), AMD1 alloy after recrystallization (b) and AMD2 alloy after recrystallization (c)

is more restricted in the ordered structures because of a higher lattice frictional force caused by ordering. On the other hand, increase in the degree of order stabilizes γ'_1 martensite which needs more stress for deformation than β'_1 martensite [23]. Nevertheless, both alloys have a β'_1 martensite type and the annealing time is 15 s for both alloys. Therefore, the higher fracture stress of AMD2 alloy is mainly caused by its smaller grain size.

Both curves after recrystallization showed the classical stress—strain curve of shape memory alloys

with an initial elastic region, then a near-plateau region, and finally a hardening regime leading to fracture (Figs. 5(b) and (c)). Region I of two curves is elastic deformation stage. The yield stress values were evaluated from curves by 0.2% offset method as (155 ± 5) MPa and (170 ± 5) MPa for AMD1 and AMD2 alloys, respectively. Region II is the regime dominated by the deformation-induced phase transformation and reorientation of martensite variants which were associated with a large recoverable strain [24]. The yield martensite variants are favorably oriented with regards to the applied stress and constraint from the neighboring grains. The region II, in two alloys is almost similar to each other, with a nearly same elongation, but a higher slope for AMD2 alloy. After recrystallization, AMD2 alloy possesses a finer grain size, and hence, has more grain boundaries. For these reasons, reorientation of martensite variants and development of deformations and slips become slower. Maybe this is the reason of higher slope of region II in AMD2 alloy compared with AMD1 alloy. Region III of the two alloys is hardening stage. In this region some further transformation occurs, and building-up of dislocation structures during plastic deformation led to strain hardening in this stage [22].

3.3 Shape memory properties

3.3.1 Transformation characteristics

Differential scanning cooling (DSC) was used to determine the transformation characteristics of recrystallized AMD1 and AMD2 alloys. Figure 6 shows the DSC curves for these two alloys. Both curves show an endothermic reaction during heating and an exothermic reaction during cooling, the endothermic reaction indicates the martensite to austenite (reverse) transformation and the exothermic reaction marks the austenite to martensite (forward) transformation. Martensitic transformation temperatures were determined from DSC curves and listed in Table 1. As shown in Fig. 6, temperatures at which the extrapolation of peaks and the base line intersect, were defined as the transformation temperature.

Table 1 indicates that martensitic transformation temperatures (M_s and M_f) of AMD1 alloy are lower than those of AMD2 alloy. In the Cu–Al–Mn SMA systems, M_s and M_f are a function of aluminum and manganese contents and decrease with increasing Al and Mn contents. In addition, Al has a greater influence on these temperatures than Mn [25]. Aluminum also has a same effect in Cu–Al–Ni SMA system. Decreasing the aluminum concentration generally leads to an increase in martensitic transformation temperatures and domination of $\beta \rightleftharpoons \beta'_1$ transformation. For AMD2 alloy, transformation shows a smooth behavior and a sharp pick during the forward and reverse transformation.

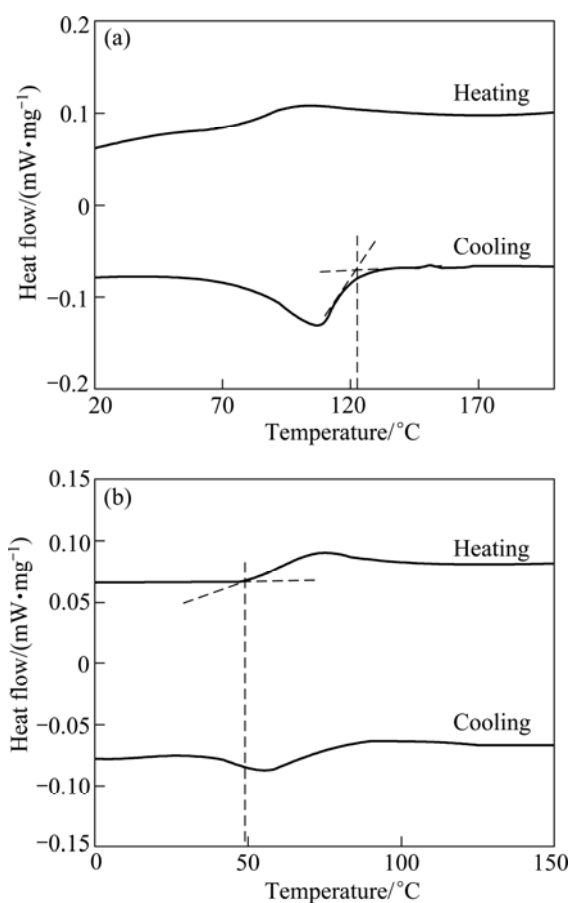


Fig. 6 DSC curves of AMD2 (a) and AMD1 (b) alloys after recrystallization

Table 2 Corrosion parameters obtained from polarization measurements of recrystallized AMD1 and AMD2 alloys

| Alloy | $\varphi_{\text{corr}}/ \text{V}$ | $J_{\text{corr}}/ (\mu\text{A}\cdot\text{cm}^{-2})$ | $\beta_{\text{a}}/ (\text{mV}\cdot\text{dec}^{-1})$ | $\beta_{\text{c}}/ (\text{mV}\cdot\text{dec}^{-1})$ | $R_{\text{p}}/ (\text{k}\Omega\cdot\text{cm}^2)$ |
|-------|-----------------------------------|---|---|---|--|
| AMD1 | -0.25 | 4.3 | 36.24 | 35.48 | 1.8 |
| AMD2 | -0.24 | 3.7 | 43.85 | 83.57 | 3.4 |

These characteristics implied that only $\beta \rightleftharpoons \beta'_1$ transformation occurred in the heating–cooling process [26]. Figure 7 (a) also shows zig-zag morphology of β'_1 martensite variants, which confirms the DSC results. However, in the case of AMD2 alloy, OM and SEM observations show the coexistence of predominant β'_1 martensite and a smaller amount of γ'_1 martensite. DSC curves of this alloy also exhibit one endothermic or exothermic sharp pick during heating or cooling, respectively, indicating that the typical one-step thermoelastic martensitic transformation occurred in the AMD1 alloy.

3.3.2 Shape memory effect (SME)

It is suggested that the shape recovery rate is not a function of grain size, but rather a function of grain size relative to the dimension of specimen (d/D , where d is

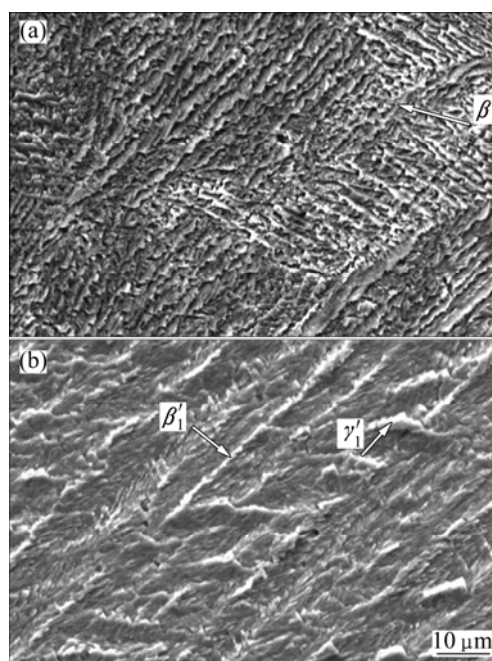


Fig. 7 SEM images of thermally-induced martensite in AMD2 (a) and AMD1 (b) alloys after recrystallization

the grain size and D is the diameter or thickness of specimen). However, in this work, the thickness of specimens was constant and so, only variations in grain size were studied. Figure 8 shows the change in shape recovery rate, η , with solution treatment time at 800 °C for AMD1 and AMD2 alloys. From Fig. 8 it can be seen that the effect of solution treatment time on η of two alloys are almost similar. Before recrystallization, η values of both alloys are 98%–100%. Once the solution treatment begins, η decreases in the first 15 s of solution treatment and then, increases with increasing solution treatment time. The minimum η is obtained after 15 s (corresponding to the minimum grain size for both alloys) as 94%–95% and 79%–80% for AMD1 and AMD2 alloys, respectively.

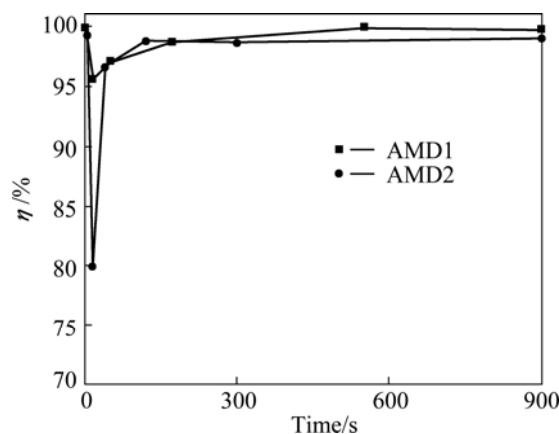


Fig. 8 Variations of shape recovery rate vs solution treatment time for AMD1 and AMD2 alloys

MALLIK and SAMPATH et al [25] explained that the strain recovery depends mainly on the amount of martensite to austenite transformation and it is not much affected by the alloy composition. Material defects such as vacancies, dislocations and other material imperfections can impede martensite transformation and thereby shape recovery. As grain size (d/D ratio) decreases, because of increasing grain constraint, more plastic deformation occurs along with martensite plate growth. This plastic deformation hampers martensite transformation and in turn strain recovery. Pervious investigations have reported the increase of shape recovery with increasing d/D ratio for Cu–Al–Ni [5], Cu–Al–Mn [20], and Cu–Al–Be [27] SMAs. It is also found that, other shape memory properties such as stress hysteresis, $\Delta\sigma$, and martensite-start stress, σ_y , decrease with increasing d/D ratio.

3.4 Corrosion behavior

The potentiodynamic polarization behaviors of alloys obtained in a potential range from -0.4 V to 0.002 V (vs Ag/AgCl) with a scan rate of 0.61 mV/s, are represented in Fig. 9. The cathodic and anodic branches of polarization curves of both alloys represent oxygen reduction and alloy dissolution, respectively. In this potential range, anodic branches of polarization curves show only the apparent Tafel region. The passivation region and the third region in which the current density increases again with the potential increasing, appear in higher potential regions [28]. The polarization resistance, R_p , can be calculated from the corrosion current density according to the Stern–Geary equation [29]:

$$R_p = \left(\frac{d\phi}{di} \right)_{i \rightarrow 0} = \frac{\beta_a \beta_b}{2.3(\beta_a + \beta_c) J_{\text{corr}}} \quad (3)$$

where β_a and β_c represent the anodic and cathodic Tafel slopes, respectively. The corrosion current density is 4.3 $\mu\text{A}/\text{cm}^2$ for AMD1 alloy, and 3.7 $\mu\text{A}/\text{cm}^2$ for AMD2 alloy, and so, polarization resistance, R_p , determined by Stern–Geary equation as 1.8 and 3.4 for AMD1 and AMD2 alloys, respectively. Other corrosion data obtained from the potentiodynamic and linear polarization measurements are presented in Table 2. It seems that corrosion resistance of AMD2 alloy is better than AMD1 alloy. This is indicated by the lower J_{corr} and higher ϕ_{corr} of AMD2 alloy compared with AMD1 alloy. Tafel slopes were obtained from linear polarization measurements which are near to 58 – 76 mV/dec [30]. However, AMD1 alloy shows more deviation from this range. Maybe this is due to the fact that Mn has a lower corrosion potential (more activity) than Cu or Ni.

Nevertheless, since copper is the main component in these Cu-based SMAs, it can be considered that the main anodic reaction is the dissolution of copper [31]. Therefore, it suggests that polarization behavior of these Cu-based SMAs in chloride solution is mainly dominated by the dissolution of copper to soluble cuprous chloride ion complex (CuCl_2^-) and its mass transport-kinetics from the electrode surface to the bulk solution [28–30].

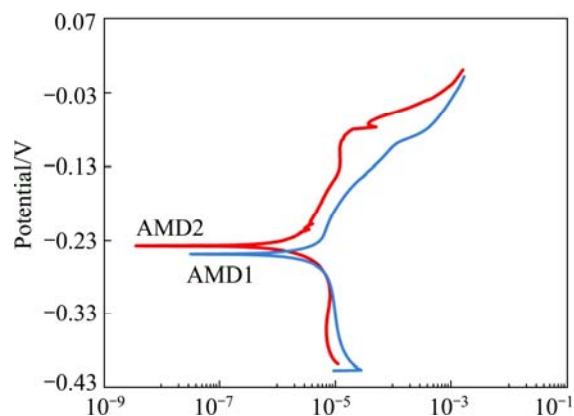


Fig. 9 Potentiodynamic polarization curves for AMD1 and AMD2 alloys in 5% NaCl (aq) solution

4 Conclusions

1) Static recrystallization of two Cu-based shape memory alloys shows a usual behavior for Cu–Al–Mn SMAs and an abnormal behavior for Cu–Al–Ni–Mn SMAs. The minimum grain sizes obtained after complete recrystallization are 260 and 90 μm for Cu–Al–Mn and Cu–Al–Ni–Mn SMAs, respectively. The kinetic exponent of Cu–Al–Ni–Mn SMA is lower than that of Cu–Al–Mn SMA (0.19 of Cu–Al–Ni–Mn alloy vs 0.38 of Cu–Al–Mn alloy). The lower grain size and kinetic exponent of Cu–Al–Ni–Mn SMA could be attributed to the Mn drag effect at grain boundaries.

2) Tensile tests show that fracture stress and strain increase after grain refinement, the highest fracture stress of 620 MPa was obtained in Cu–Al–Ni–Mn SMAs. The maximum fracture strain for both alloys is almost 11% .

3) For AMD2 alloy, DSC curves show a smooth behavior with an endothermic and exothermic pick during heating and cooling, respectively. These characteristics indicate that only $\beta \rightleftharpoons \beta'_1$ occurs in the reverse and forward transformation. Nevertheless, OM and SEM observations of AMD1 alloy show the coexistence of predominant β'_1 martensite and a smaller amount of γ'_1 martensite.

4) Shape recovery rate (η) values increase with increasing d/D ratio. The minimum η values obtained after 15 s of solution treatment time are 79% – 80% and

94%–95% for Cu–Al–Ni–Mn and Cu–Al–Mn SMAs, respectively.

5) Cu–Al–Ni–Mn alloy exhibits a lower J_{corr} of 3.7 $\mu\text{A}/\text{cm}^2$ vs 4.3 $\mu\text{A}/\text{cm}^2$ and higher ϕ_{corr} of -0.24 vs -0.25 than Cu–Al–Mn SMA. Tafel slopes are near to 58–76 mV/dec, with a more deviation from this range for Cu–Al–Mn SMA. It is suggested that anodic reactions are dominated by dissolution of copper.

References

- [1] MORGAN N B. Medical shape memory alloy applications—The market and its products [J]. *Mater Sci Eng A*, 2004, 378: 16–23.
- [2] SONG G, MA N, LI H N. Applications of shape memory alloys in civil structures [J]. *Eng Struct*, 2006, 28: 1266–1274.
- [3] van HUMBEECK J. Non-medical applications of shape memory alloys [J]. *Mater Sci Eng A*, 1999, 273–275: 134–148.
- [4] TADAKI T. Cu-based shape memory alloys [C]//OTSUKA K, WAYMAN C M. *Shape Memory Materials*. United Kingdo: Cambridge University Press, 1998: 97–116.
- [5] SURE G N, BROWN L C. The mechanical properties of grain refined β -CuAlNi strain-memory alloys [J]. *Metall Trans A*, 1984, 15: 1613–1621.
- [6] KIM DWR J W, LEE E S, KIM Y G. Effects on microstructure and tensile properties of a zirconium addition to a Cu–Al–Ni shape memory alloy [J]. *Metall Trans A*, 1990, 21: 741–744.
- [7] ROH D W, KIM J W, CHO T J, KIM Y G. Tensile properties and microstructure of microalloyed Cu–Al–Ni–X shape memory alloys [J]. *Mater Sci Eng A*, 1991, 136: 17–23.
- [8] MORRIS M A. High temperature properties of ductile Cu–Al–Ni shape memory alloys with boron additions [J]. *Acta Metall Mater*, 1992, 40: 1573–1586.
- [9] MORRIS M A, LIPE T. Microstructural influence of Mn additions on thermoelastic and pseudoelastic properties of Cu–Al–Ni alloys [J]. *Acta Metall Mater*, 1994, 42: 1583–1594.
- [10] KAINUMA R, TAKAHASHI S, ISHIDA K. Thermoelastic martensite and shape memory effect in ductile Cu–Al–Mn alloys [J]. *Metall Mater Trans A*, 1996, 27: 2187–2195.
- [11] SUTOU Y, OMORI T, KAINUMA R, ONO N, ISHIDA K. Enhancement of superelasticity in Cu–Al–Mn–Ni shapememory alloys by texture control [J]. *Metall Mater Trans A*, 2002, 33: 2817–2824.
- [12] SUTOU Y, KOEDA N, OMORI T, KAINUMA R, ISHIDA K. Effects of ageing on bainitic and thermally induced martensitic transformations in ductile Cu–Al–Mn-based shape memory alloys [J]. *Acta Mater*, 2009, 57: 5748–5758.
- [13] SUTOU Y, KOEDA N, OMORI T, KAINUMA R, ISHIDA K. Effects of aging on stress-induced martensitic transformation in ductile Cu–Al–Mn-based shape memory alloys [J]. *Acta Mater*, 2009, 57: 5759–5770.
- [14] MALLIK U S, SAMPATH V. Effect of alloying on microstructure and shape memory characteristics of Cu–Al–Mn shape memory alloys [J]. *Mater Sci Eng A*, 2008, 481–482: 680–683.
- [15] SUTOU Y, KAINUMA R, ISHIDA K. Effect of alloying elements on the shape memory properties of ductile Cu–Al–Mn alloys [J]. *Mater Sci Eng A*, 1999, 273–275: 375–379.
- [16] SUTOU Y, OMORI T, KOEDA N, KAINUMA R, ISHIDA K. Effects of grain size and texture on damping properties of Cu–Al–Mn-based shape memory alloys [J]. *Mater Sci Eng A*, 2006, 438–440: 743–746.
- [17] MALLIK U S, SAMPATH V. Effect of composition and ageing on damping characteristics of Cu–Al–Mn shape memory alloys [J]. *Mater Sci Eng A*, 2008, 478: 48–55.
- [18] JIAO Y Q, WEN Y H, LI N, HE J Q, TENG J. Effect of solution treatment on damping capacity and shape memory effect of a CuAlMn alloy [J]. *J Alloys Compd*, 2010, 491: 627–630.
- [19] WANG R, GUI J, CHEN X, TAN S. EBSD and TEM study of self-accommodating martensites in Cu_{75.7}Al_{15.4}Mn_{8.9} shape memory alloy [J]. *Acta Mater*, 2002, 50: 1835–1847.
- [20] SUTOU Y, OMORI T, YAMAUCHI K, ONO N, KAINUMA R, ISHIDA K. Effect of grain size and texture on pseudoelasticity in Cu–Al–Mn-based shape memory wire [J]. *Acta Mater*, 2005, 53: 4121–4133.
- [21] GIL F J, GUILLEMANY J M, FERNÁNDEZ J. Kinetic grain growth in β -copper shape memory alloys [J]. *Mater Sci Eng A*, 1998, 241: 114–121.
- [22] SARI U, KIRINDI T. Effects of deformation on microstructure and mechanical properties of a Cu–Al–Ni shape memory alloy [J]. *Mater Charact*, 2008, 59: 920–929.
- [23] PICORNELL C, PONS J, CESARI K E. Stabilisation of martensite by applying compressive stress in Cu–Al–Ni single crystals [J]. *Acta Mater*, 2001, 49: 4221–4230.
- [24] HUANG W M, WU J A, LIM B Y, VAHMI I E. V-shape in Young's modulus versus strain relationship in shape memory alloys upon mechanical loading [J]. *J Alloys Compd*, 2005, 390: 175–181.
- [25] MALLIK U S, SAMPATH V. Influence of aluminum and manganese concentration on the shape memory characteristics of Cu–Al–Mn shape memory alloys [J]. *J Alloys Compd*, 2008, 459: 142–147.
- [26] RECARTE V, PEREZ-SAEZ R B, BOCANEGRA E H, NO M L, SAN JUAN J. Influence of Al and Ni concentration on the martensitic transformation in Cu–Al–Ni shape-memory alloys [J]. *Metall Mater Trans A*, 2002, 33: 2581–2591.
- [27] MONTECINOS S, CUNIBERTI A, SEPÚLVEDA A. Grain size and pseudoelastic behaviour of a Cu–Al–Be alloy [J]. *Mater Charact*, 2008, 59: 117–123.
- [28] GOJIĆ M, VRSALLOVIĆ L, KOŽUH S, KNEISSL A, ANŽEL I, GUDIĆ S, KOSEC B, KLISKIC M. Electrochemical and microstructural study of Cu–Al–Ni shape memory alloy [J]. *J Alloys Compd*, 2011, 509: 9782–9790.
- [29] BADAWY W A, EL-SHERIF R M, SHEHATA H. Electrochemical stability of Cu–10Al–5Ni alloy in chloride–sulfate electrolytes [J]. *Electrochim Acta*, 2009, 54: 4501–4505.
- [30] ALFANTAZI A M, AHMED T M, TROMANS D. Corrosion behavior of copper alloys in chloride media [J]. *Materials & Design*, 2009, 30: 2425–2430.
- [31] HURTADO M R F, SUMODJO P T A, BENEDETTI A V. Electrochemical studies with a Cu–5wt.%Ni alloy in 0.5 M H₂SO₄ [J]. *Electrochim Acta*, 2003, 48: 2791–2798.

经形变热处理铜基形状记忆合金的 晶粒生长、形状记忆和腐蚀行为

Ahmad Ostovari MOGHADDAM, Mostafa KETABCHI, Reza BAHRAMI

Department of Mining and Metallurgical Engineering, Amirkabir University of Technology, Tehran, Iran

摘要: 比较研究了 Cu-11.8% Al-3.7% Ni-1% Mn 和 Cu-11% Al-5.6% Mn 形状记忆合金(SMAS)的形状记忆、腐蚀性能。采用光学显微镜(OM)、扫描电子显微镜(SEM)、差示扫描量热法(DSC)、动电位极化、弯曲和拉伸试验,研究了晶粒细化对这些性能的影响。在 800 °C 退火时,在首先的 15 s 内静态再结晶和动态晶粒长大显示出一个快速的再结晶过程,随后才是晶粒生长。退火 15 s 后得到的 Cu-Al-Ni-Mn 和 Cu-Al-Mn 合金的最小晶粒尺寸分别为 90 μm 和 260 μm 。拉伸试验表明 2 种合金呈现典型的三阶段曲线,由此可以看出,晶粒细化后合金具有高的断裂应力和应变。显微组织表明,Cu-Al-Ni-Mn 合金中存在锯齿状的 β_1' 马氏体形态,通过差示扫描量热法也证实了 β_1' 和 γ_1' 共存于 Cu-Al-Mn 合金中。评估了形变热处理前、后及 800 °C 退火 15 min,随后进行水淬的合金的形状记忆性能。另外,采用动电位极化法分析了晶粒细化后合金的腐蚀行为。结果表明,铜溶解过程中主要为阳极反应,Cu-Al-Ni-Mn 合金比 Cu-Al-Mn 合金具有更好的耐腐蚀性。

关键词: 形状记忆合金(SMAs); 晶粒细化; 腐蚀; 形状记忆性能

(Edited by Xiang-qun LI)